This article has been accepted for publication in IEEE Communications Letters. This is the author's version which has not been fully edited and content may change prior to final publication. Citation information: DOI 10.1109/LCOMM.2022.3181728

General Form of the Power Spectral Density of Multicarrier Signals

Roberto López-Valcarce, *Senior Member, IEEE*

***Abstract*— Multicarrier modulation has been adopted in many modern communication systems because of its many appealing properties. Its relatively high out-of-band radiation has spurred many techniques to shape the power spectral density (PSD) of multicarrier signals, including spectral precoding and pulse shaping. We derive a general expression for the PSD which is valid for subcarrier-specific pulses and for spectral precoders operating over multiple blocks. The only statistical assumptions on the vector-valued sequence modulating the active subcarriers are wide-sense cyclostationarity and properness. The applicability of the result to a number of popular multicarrier formats is discussed.**

***Index Terms*— Multicarrier modulation, OFDM, GFDM, OTFS, power spectral density.**

I. Introduction

The many appealing properties of multicarrier modulation, e.g., robustness against frequency selective channels, receiver simplicity, and good matching with multiple-input multiple-output (MIMO) operation, have made it the format of choice in many communication standards. Multicarrier systems transmit information block by block, with each block generated with an inverse discrete Fourier transform (IDFT) operation, and with consecutive blocks separated by some form of guard interval to avoid intersymbol interference [1].

The power spectral density (PSD) of communication signals is an important function in system design, as it determines the degree of compliance to limits imposed by spectral emission masks. Spectral precoding and pulse shaping are popular techniques to shape the PSD of multicarrier signals in order to reduce their relatively large out-of-band radiation and improve spectrum usage [2], [3]. Over the years, many variants of these techniques have been proposed, and it is important to have accurate expressions for the PSD of the multicarrier signal for a practical assessment of their performance.

A number of expressions for the PSD of multicarrier signals can be found in the literature, but they are only valid under particular assumptions such as rectangular pulse shaping [4], [5], negligible effect of the IDFT-based implementation [6], [7], statistical independence of data across subcarriers [8], or across blocks [9]. These assumptions do not apply to many spectral shaping techniques, in which pulses need not be rectangular [10]–[12] or even vary across subcarriers [13]; similarly, precoding operations on the modulating data introduce correlation across subcarriers in a given block [14]–[20], or even across different blocks [21]–[25]. In this letter we provide a detailed derivation of the PSD of the multicarrier signal, under the only assumption of a zero-mean, wide-sense cyclostationary and proper vector-valued sequence modulating the active subcarriers. In contrast with the standard assumption that different blocks be uncorrelated, we still allow for inter-block correlation, so that we encompass precoding operations over more than one block. Besides providing insights into the influence of the different system parameters, with the expressions derived herein signal generation and spectral estimation can be avoided when evaluating the PSD.

The author is with atlanTTic (Research Center in Telecommunications), Universidade de Vigo, Vigo, Spain. Email: valcarce@gts.uvigo.es

This work was funded by MCIN/ AEI/10.13039/501100011033/ FEDER "Una manera de hacer Europa" under project RODIN (PID2019-105717RB-C21).

II. Signal model

Consider a multicarrier signal generated with an IDFT of size N. Let $\mathcal{K} = \{k_1, k_2, \ldots, k_K\}$ denote the set of indices of active subcarriers, and let $x_k^{(m)}$ be the data modulated on the k-th subcarrier in the m-th block. The baseband samples of the multicarrier signal are then given by

$$s[n] = \sum_{m=-\infty}^{\infty} \sum_{k \in \mathcal{K}} x_k^{(m)} h_k[n - mL] \mathrm{e}^{\jmath \frac{2\pi}{N} k(n-mL)}, \quad (1)$$

where L is the hop size in samples, and $h_k[n]$ is the shaping pulse for the k-th subcarrier, with Fourier transform

$$H_k(\mathrm{e}^{\jmath\omega}) = \sum_{n=-\infty}^{\infty} h_k[n] \mathrm{e}^{-\jmath\omega n}. \quad (2)$$

We allow for general shaping pulses $h_k[n]$. This encompasses a number of cases from the literature, including cyclic prefix (CP), zero padding (ZP) and windowing (W) OFDM; the application to more advanced multicarrier formats, i.e., Generalized Frequency Division Multiplexing (GFDM), Orthogonal Time-Frequency-Space (OTFS) and Offset-QAM Filterbank Multicarrier (OQAM-FBMC) is discussed in Sec. V.

1) **CP-OFDM.** All subcarriers use the same length-L rectangular pulse shape: for all k, $h_k[n] = 1$ for $0 \leq n \leq L-1$ and zero otherwise. The CP length is $L-N$ samples: for all p integer, the baseband samples (1) satisfy $s[pL+q] = s[pL+q+N]$, $0 \leq q \leq L-N-1$.
2) **ZP-OFDM.** All subcarriers use the same length-N rectangular pulse shape: for all k, $h_k[n] = 1$ for $L-N \leq n \leq L-1$ and zero otherwise. The ZP guard interval length is $L-N$ samples.
3) **W-OFDM.** All subcarriers use the same pulse: for all k, $h_k[n] = h_0[n] = 1$ for $Q \leq n \leq L-1$ and $h_0[n] = 0$ for $n < 0$ and $n \geq L+Q$. For $0 \leq n \leq Q-1$ and $L \leq n \leq L+Q-1$, the values of $h_0[n]$ smoothly transition between 0 and 1 [10]. There are Q overlapping samples between consecutive blocks. These overlapping samples are discarded at the receiver, and the effective CP length is $L-N-Q$. For $Q=0$, W-OFDM reduces to CP-OFDM.
4) **Edge Windowing.** In this generalization of W-OFDM, each subcarrier is assigned its own pulse $h_k[n]$ and

overlapping factor Q_k [13]. The hop size is common to all subcarriers, so that the effective CP length for subcarrier k is $L-N-Q_k$. In its most common form, two groups (*inner* and *edge* subcarriers) are formed, and the same pulse is assigned to all subcarriers in the same group.

The baseband continuous-time multicarrier signal is obtained as the output of a digital-to-analog converter (DAC) with sampling frequency $f_s = \frac{1}{T_s}$ when the input is $s[n]$:

$$s(t) = \sum_{n=-\infty}^{\infty} s[n] h_{\rm I}(t - nT_s), \tag{3}$$

where $h_{\rm I}(t)$ is the impulse response of the interpolation filter in the DAC, with Fourier transform $H_{\rm I}(f) = \int_{-\infty}^{\infty} h_{\rm I}(t) {\rm e}^{-\jmath 2\pi f t} {\rm d}t$. The subcarrier spacing (in Hz) is then given by $\Delta_f = \frac{1}{NT_s}$. The bandpass signal is obtained as

$$\tilde{s}(t) = {\rm Re}\{s(t) {\rm e}^{\jmath 2\pi f_c t}\}, \tag{4}$$

where f_c is the carrier frequency.

The following assumption will be adopted; basically, it states that the complex-valued sequences modulating the different subcarriers are jointly wide-sense stationary and proper.

Assumption 1: Let $\boldsymbol{x}_m = \left[\begin{array}{cccc} x_{k_1}^{(m)} & x_{k_2}^{(m)} & \cdots & x_{k_K}^{(m)} \end{array} \right]^T$. Then (i) $\mathbb{E}\{\boldsymbol{x}_m\} = \boldsymbol{0}$, (ii) $\mathbb{E}\{\boldsymbol{x}_m \boldsymbol{x}_{m-\ell}^T\} = \boldsymbol{0}$ for all (m, ℓ), and (iii) $\mathbb{E}\{\boldsymbol{x}_m \boldsymbol{x}_{m-\ell}^H\}$ depends on ℓ only, but not on m.

Under Assumption 1, the PSD matrix of the vector-valued process $\{\boldsymbol{x}_m\}$ is denoted as

$$\boldsymbol{S}_{\boldsymbol{x}}(f) = \sum_{\ell} \mathbb{E}\{\boldsymbol{x}_m \boldsymbol{x}_{m-\ell}^H\} {\rm e}^{-\jmath 2\pi f T_s \ell}. \tag{5}$$

III. Power Spectral Density

Our main result can be stated as follows.

Theorem 1: Let us define the vector

$$\boldsymbol{\phi}(f) \triangleq \left[\begin{array}{cccc} \phi_{k_1}(f) & \phi_{k_2}(f) & \cdots & \phi_{k_K}(f) \end{array} \right]^T, \tag{6}$$

where $\phi_k(f) \triangleq H_k^* \left({\rm e}^{\jmath 2\pi (f - k\Delta_f) T_s} \right)$. Then, the PSD of the baseband multicarrier signal $s(t)$ in (3) is given by

$$S_s(f) = \frac{|H_{\rm I}(f)|^2}{LT_s} \boldsymbol{\phi}^H(f) \boldsymbol{S}_{\boldsymbol{x}}(Lf) \boldsymbol{\phi}(f). \tag{7}$$

Expression (7) reveals the influence of the three elements featuring in the synthesis of the multicarrier signal (3):

- **Interpolation filter.** The effect of this lowpass filter is to remove the undesired replicas present in the term $\boldsymbol{\phi}^H(f) \boldsymbol{S}_{\boldsymbol{x}}(Lf) \boldsymbol{\phi}(f)$, which is periodic in f with period equal to the sampling rate f_s.
- **Shaping pulse.** The shaping pulses affect the vector $\boldsymbol{\phi}(f)$, whose entries are shifted replicas of (the conjugate of) their transfer functions to the positions of the active subcarriers $\{k\Delta_f \,|\, k \in \mathcal{K}\}$. If the same pulse $h_0[n]$ is used for all subcarriers, then $\phi_k(f) = \phi_0(f - k\Delta_f)$ with $\phi_0(f) = H_0^* \left({\rm e}^{\jmath 2\pi f T_s} \right)$. One has

$$\phi_0(f) = L \frac{{\rm sinc}(fT_s L)}{{\rm sinc}(fT_s)} {\rm e}^{\jmath \pi f T_s (L-1)} \quad \text{(CP-OFDM)}, \tag{8}$$

$$\phi_0(f) = N \frac{{\rm sinc}(fT_s N)}{{\rm sinc}(fT_s)} {\rm e}^{\jmath \pi f T_s (N-1)} \quad \text{(ZP-OFDM)}, \tag{9}$$

whereas for W-OFDM, $\phi_0(f)$ depends on the particular window used.

- **Precoding.** The matrix PSD $\boldsymbol{S}_{\boldsymbol{x}}(Lf)$ can be designed to shape the transmitted signal PSD (7) via precoding. The transmitted vector sequence $\{\boldsymbol{x}_m \in \mathbb{C}^K\}$ is obtained from the data sequence $\{\boldsymbol{d}_m \in \mathbb{C}^D\}$, with $K \geq D$; a precoder is a mapping from $\{\boldsymbol{d}_m\}$ to $\{\boldsymbol{x}_m\}$, with rate $\frac{D}{K} \leq 1$. Usually the data sequence is zero-mean and uncorrelated, with $\mathbb{E}\{\boldsymbol{d}_m \boldsymbol{d}_{m-\ell}^H\} = \delta[\ell] \boldsymbol{I}_D$. For a memoryless linear precoder, $\boldsymbol{x}_m = \boldsymbol{G}_0 \boldsymbol{d}_m$, with $\boldsymbol{G}_0 \in \mathbb{C}^{K \times D}$ the precoding matrix, and $\boldsymbol{S}_{\boldsymbol{x}}(f) = \boldsymbol{G}_0 \boldsymbol{G}_0^H$ becomes frequency-independent. For example, in DFT-s-OFDM [26] one has $K = D$, and $\boldsymbol{G}_0$ is the $D \times D$ DFT matrix; since $\boldsymbol{G}_0 \boldsymbol{G}_0^H = \boldsymbol{I}_D$, it is seen that DFT spreading does not affect the PSD.
  More generally, if the precoder is a linear time-invariant (LTI) filter, i.e., $\boldsymbol{x}_m = \sum_\ell \boldsymbol{G}_\ell \boldsymbol{d}_{m-\ell}$, then $\boldsymbol{S}_{\boldsymbol{x}}(f) = \boldsymbol{G}(f) \boldsymbol{G}^H(f)$, with $\boldsymbol{G}(f) = \sum_\ell \boldsymbol{G}_\ell {\rm e}^{-\jmath 2\pi f T_s \ell}$. Note that the argument of $\boldsymbol{S}_{\boldsymbol{x}}(Lf)$ in (7) is affected by the hop size L, so that $\boldsymbol{S}_{\boldsymbol{x}}(Lf)$ is $\frac{f_s}{L}$-periodic in f. Hence, this function cannot be freely specified over the range $|f| \leq \frac{f_s}{2}$, an effect that limits spectral precoder performance.

IV. Proof of Theorem 1

To prove Theorem 1, we proceed in six steps. In essence, $s(t)$ is shown to be cyclostationary, so that its PSD is the Fourier transform of its averaged autocorrelation function.

Step 1. First, note that under Assumption 1, the discrete-time process $\{s[n]\}$ in (1) is zero-mean wide-sense cyclostationary with period L, i.e., $R_s[n,d] \triangleq \mathbb{E}\{s^*[n] s[n+d]\}$ satisfies $R_s[n+L,d] = R_s[n,d]$ for all n and d. To see this, let $R_x[k,k';m'-m] \triangleq \mathbb{E}\left\{ \left(x_k^{(m)} \right)^* x_{k'}^{(m')} \right\}$; then one has

$$\begin{aligned} R_s[n,d] &= \sum_m \sum_{m'} \sum_{k \in \mathcal{K}} \sum_{k' \in \mathcal{K}} R_x[k,k';m'-m] \\ &\quad \times h_k^*[n - mL] h_{k'}[n + d - m'L] \\ &\quad \times {\rm e}^{-\jmath \frac{2\pi}{N} k(n-mL)} {\rm e}^{\jmath \frac{2\pi}{N} k'(n+d-m'L)}, \end{aligned} \tag{10}$$

which is L-periodic in n. From Assumption 1 it also follows that $\mathbb{E}\left\{ x_k^{(m)} x_{k'}^{(m')} \right\} = 0$ for all k, k', m, m', so that the process $\{s[n]\}$ is proper: its pseudo-autocorrelation $P_s[n,d] \triangleq \mathbb{E}\{s[n] s[n+d]\}$ is zero for all n and d.

Step 2. The above properties of $\{s[n]\}$ translate into similar ones for the continuous-time baseband signal $s(t)$. Letting $R_s(t,\tau) \triangleq \mathbb{E}\{s^*(t) s(t+\tau)\}$, it is readily checked that $R_s[n+L,d] = R_s[n,d]$ implies $R_s(t+LT_s,\tau) = R_s(t,\tau)$, whereas $P_s[n,d] = 0$ implies $P_s(t,\tau) \triangleq \mathbb{E}\{s(t) s(t+\tau)\} = 0$ for all t and τ. Therefore, the process $s(t)$ is proper and wide-sense cyclostationary with period LT_s.

Step 3. Now we show that the averaged autocorrelation of $s(t)$, i.e., $R_s(\tau) \triangleq \frac{1}{LT_s} \int_0^{LT_s} R_s(t,\tau) {\rm d}t$, is given by

$$R_s(\tau) = \frac{1}{T_s} \sum_d R_s[d] g_{\rm I}(\tau - dT_s), \tag{11}$$

where $R_s[d] \triangleq \frac{1}{L} \sum_{n=0}^{L-1} R_s[n,d]$ is the averaged autocorrelation of $\{s[n]\}$, and $g_{\rm I}(\tau) \triangleq \int_{-\infty}^{\infty} h_{\rm I}^*(t) h_{\rm I}(t+\tau) {\rm d}t$ is

This article has been accepted for publication in IEEE Communications Letters. This is the author's version which has not been fully edited and content may change prior to final publication. Citation information: DOI 10.1109/LCOMM.2022.3181728

the autocorrelation function of the interpolation pulse, with Fourier transform $|H_{\rm I}(f)|^2$. Averaging $R_s(t,\tau)$, one has

$$\begin{aligned} R_s(\tau) &= \frac{1}{LT_s}\sum_n\sum_d R_s[n,d]\int_0^{LT_s} h_{\rm I}^*(t-nT_s) \\ &\quad \times h_{\rm I}(t+\tau-(n+d)T_s){\rm d}t. \end{aligned} \tag{12}$$

Writing $n=p+qL$, with p,q integers and $0\le p\le L-1$, and using the fact that $R_s[p+qL,d]=R_s[p,d]$, (11) follows.

Step 4. Taking the Fourier transform of (11), the PSD of the cyclostationary process $s(t)$ is obtained:

$$S_s(f)=\frac{|H_{\rm I}(f)|^2}{T_s}\cdot\sum_d R_s[d]{\rm e}^{-j2\pi fT_sd}. \tag{13}$$

Step 5. Now we must obtain $R_s[d]$, taking (1) into account:

$$\begin{aligned} R_s[d] &= \sum_m\sum_{m'}\sum_{k\in\mathcal{K}}\sum_{k'\in\mathcal{K}} R_x[k,k';m'-m] \\ &\quad\times\frac{1}{L}\sum_{n=0}^{L-1} h_k^*[n-mL]h_{k'}[n+d-m'L] \\ &\quad\times{\rm e}^{-\jmath\frac{2\pi}{N}k(n-mL)}{\rm e}^{\jmath\frac{2\pi}{N}k'(n+d-m'L)} \qquad (14) \\ &= \sum_m\sum_b\sum_{k\in\mathcal{K}}\sum_{k'\in\mathcal{K}} R_x[k,k';b]{\rm e}^{\jmath\frac{2\pi}{N}k'(d-bL)} \\ &\quad\times\frac{1}{L}\sum_{n=0}^{L-1} h_k^*[n-mL]h_{k'}[n+d-(m+b)L] \\ &\quad\times{\rm e}^{-\jmath\frac{2\pi}{N}(k-k')(n-mL)}. \qquad (15) \end{aligned}$$

Letting now $q=n-mL$, (15) becomes

$$\begin{aligned} R_s[d] &= \sum_b\sum_{k\in\mathcal{K}}\sum_{k'\in\mathcal{K}} R_x[k,k';b]{\rm e}^{\jmath\frac{2\pi}{N}k'(d-bL)} \\ &\quad\times\frac{1}{L}\sum_q h_k^*[q]h_{k'}[q+d-bL]{\rm e}^{-\jmath\frac{2\pi}{N}(k-k')q}. \end{aligned} \tag{16}$$

The summation over q featuring in (16) is the Fourier transform of the product $h_k^*[n]h_{k'}^*[n+d-bL]$, evaluated at $\omega=\frac{2\pi}{N}(k-k')$, and hence it is given by the circular convolution of the Fourier transforms of the factors. Since

$$\begin{aligned} h_k^*[n] &\leftrightarrow H_k^*({\rm e}^{-\jmath\omega}), \qquad (17) \\ h_{k'}[n+d-bL] &\leftrightarrow H_{k'}({\rm e}^{\jmath\omega}){\rm e}^{\jmath\omega(d-bL)}, \qquad (18) \end{aligned}$$

it follows that

$$\begin{aligned} &\sum_q h_k^*[q]h_{k'}[q+d-bL]{\rm e}^{-\jmath\omega q} \\ &\quad= \frac{1}{2\pi}\int_{-\pi}^{\pi} H_k^*({\rm e}^{-\jmath\alpha})H_{k'}({\rm e}^{\jmath(\omega-\alpha)}){\rm e}^{\jmath(\omega-\alpha)(d-bL)}{\rm d}\alpha, \end{aligned} \tag{19}$$

and therefore

$$\begin{aligned} R_s[d] &= \frac{1}{2\pi L}\sum_b\sum_{k\in\mathcal{K}}\sum_{k'\in\mathcal{K}} R_x[k,k';b]{\rm e}^{\jmath\frac{2\pi}{N}k(d-bL)} \\ &\quad\times\int_{-\pi}^{\pi} H_k^*({\rm e}^{-\jmath\alpha})H_{k'}({\rm e}^{\jmath(\frac{2\pi}{N}(k-k')-\alpha)}){\rm e}^{-\jmath\alpha(d-bL)}{\rm d}\alpha. \end{aligned} \tag{20}$$

Step 6. Using (20), the desired term featuring in (13) is given by

$$\begin{aligned} \sum_d R_s[d]{\rm e}^{-j2\pi fT_sd} &= \frac{1}{2\pi L}\sum_b\sum_{k\in\mathcal{K}}\sum_{k'\in\mathcal{K}} R_x[k,k';b] \\ &\quad\times\int_{-\pi}^{\pi} H_k^*({\rm e}^{-\jmath\alpha})H_{k'}({\rm e}^{\jmath(\frac{2\pi}{N}(k-k')-\alpha)}) \\ &\quad\times\left[\sum_d {\rm e}^{\jmath\left(\frac{2\pi}{N}k-\alpha-2\pi fT_s\right)d}\right]{\rm e}^{-\jmath\left(\frac{2\pi}{N}k-\alpha\right)bL}{\rm d}\alpha. \end{aligned} \tag{21}$$

The term in brackets in (21) is obtained by using the Fourier series representation of a comb function: $\sum_\ell\delta(t-\ell T)=\frac{1}{T}\sum_n {\rm e}^{\jmath\frac{2\pi}{T}nt}$, where $\delta(\cdot)$ is Dirac's delta function. Then

$$\sum_d {\rm e}^{\jmath\left(\frac{2\pi}{N}k-\alpha-2\pi fT_s\right)d}=2\pi\sum_\ell\delta\left(\frac{2\pi}{N}k-\alpha-2\pi fT_s-2\pi\ell\right). \tag{22}$$

Note now that for any 2π-periodic function $f(\alpha)$ it holds that

$$\sum_\ell\int_{-\pi}^{\pi} f(\alpha)\delta(\theta-\alpha-2\pi\ell){\rm d}\alpha=f(\theta). \tag{23}$$

Thus, since $H_k^*({\rm e}^{-\jmath\alpha})H_{k'}({\rm e}^{\jmath(\frac{2\pi}{N}(k-k')-\alpha)}){\rm e}^{-\jmath\left(\frac{2\pi}{N}k-\alpha\right)bL}$ is 2π-periodic in α, substituting (22) in (21), one has

$$\begin{aligned} \sum_d R_s[d]{\rm e}^{-j2\pi fT_sd} &= \frac{1}{L}\sum_b\sum_{k\in\mathcal{K}}\sum_{k'\in\mathcal{K}} R_x[k,k';b] \\ &\quad\times H_k^*({\rm e}^{\jmath2\pi(fT_s-\frac{k}{N})})H_{k'}({\rm e}^{\jmath2\pi(fT_s-\frac{k'}{N})}){\rm e}^{-\jmath2\pi fT_sbL} \\ &= \frac{1}{L}\sum_{k\in\mathcal{K}}\sum_{k'\in\mathcal{K}}\left[\sum_b R_x[k,k';b]{\rm e}^{-\jmath2\pi fT_sbL}\right]\phi_k(f)\phi_{k'}^*(f) \\ &= \frac{1}{L}\boldsymbol{\phi}^H(f)\boldsymbol{S}_{\boldsymbol{x}}(Lf)\boldsymbol{\phi}(f), \end{aligned} \tag{24}$$

which yields the desired result after substitution in (13). ■

Remark 1. Suppose we replace part (iii) of Assumption 1 by $\mathbb{E}\{\boldsymbol{x}_m\boldsymbol{x}_{m-\ell}^H\}$ being M-periodic in m. Then the expression (7) for the PSD of $s(t)$ remains valid; the only difference is that the PSD of the wide-sense *cyclostationary* and proper vector-valued process $\{\boldsymbol{x}_m\}$ is defined now as

$$\boldsymbol{S}_{\boldsymbol{x}}(f)=\sum_\ell\left(\frac{1}{M}\sum_{m=0}^{M-1}\mathbb{E}\{\boldsymbol{x}_m\boldsymbol{x}_{m-\ell}^H\}\right){\rm e}^{-\jmath2\pi fT_s\ell}. \tag{25}$$

The proof follows the same steps as above, *mutatis mutandis,* so it is skipped for brevity.

Remark 2. Consider the bandpass signal $\tilde{s}(t)$ from (4). It is clearly zero-mean, and since $P_s(t,\tau)=0$ for all t,τ, its autocorrelation reduces to

$$\begin{aligned} R_{\tilde{s}}(t,\tau) &\triangleq \mathbb{E}\{s(t+\tau)s(t)\} \\ &= \frac{1}{4}\left[R_s(t,\tau){\rm e}^{\jmath2\pi f_c\tau}+R_s^*(t,\tau){\rm e}^{-\jmath2\pi f_c\tau}\right], \end{aligned} \tag{26}$$

which is LT_s-periodic in t. Hence, the bandpass signal is wide-sense cyclostationary, and its PSD is given by

$$S_{\tilde{s}}(f)=\frac{1}{4}\left[S_s(f-f_c)+S_s(-f-f_c)\right]. \tag{27}$$

Note that (26)-(27) need not hold if $s(t)$ is not proper.

This article has been accepted for publication in IEEE Communications Letters. This is the author's version which has not been fully edited and content may change prior to final publication. Citation information: DOI 10.1109/LCOMM.2022.3181728

V. Extension to other modulation formats

A. GFDM

In GFDM, transmission is organized in terms of P sub-blocks, with different pulses being used for different subblocks [27]. Thus, (1) is replaced by

$$s[n] = \sum_{m=-\infty}^{\infty} \sum_{k\in\mathcal{K}} \sum_{p=0}^{P-1} x_{k,p}^{(m)} g_p[n-mL] \mathrm{e}^{\jmath \frac{2\pi}{N} k(n-mL)}, \quad (28)$$

with $x_{k,p}^{(m)}$ the data modulated on the k-th subcarrier of the p-th subblock of the m-th block. The pulses are usually obtained as cyclic shifts of an NP-length prototype pulse $g[n]$, $0 \le n \le NP-1$, with the insertion of a cyclic prefix of $L-NP$ samples: $g_p[n] = g[((n-pN-L))_{NP}]$ for $0 \le n \le L-1$.

Note that (28) is the superposition of P sequences $s_p[n]$, $0 \le p \le P-1$, all with the same structure as (1), but with different pulses $g_p[n]$ (common to all subcarriers for a given p). Hence, if $x_{k,p}^{(m)}$ and $x_{k',p'}^{(m')}$ are proper, and uncorrelated for all k, k', m, m' when $p \neq p'$, then the PSD of the GFDM signal is given by the sum of the corresponding P individual PSDs, each of which can be computed via (7).

B. OTFS

OTFS can be seen as a particular instance of CP-OFDM with precoding across multiple blocks [28]. Specifically, the data sequence $\{\boldsymbol{d}_m \in \mathbb{C}^K\}$ is organized in time-frequency frames $\boldsymbol{D}_q = \begin{bmatrix} \boldsymbol{d}_{qP} & \boldsymbol{d}_{qP+1} & \cdots & \boldsymbol{d}_{qP+P-1} \end{bmatrix} \in \mathbb{C}^{K\times P}$, and the corresponding frame for the transmit sequence is obtained by the inverse symplectic finite Fourier transform as $\boldsymbol{X}_q = \begin{bmatrix} \boldsymbol{x}_{qP} & \boldsymbol{x}_{qP+1} & \cdots & \boldsymbol{x}_{qP+P-1} \end{bmatrix} = \boldsymbol{F}_K \boldsymbol{D}_q \boldsymbol{F}_P^H \in \mathbb{C}^{K\times P}$, where $\boldsymbol{F}_M \in \mathbb{C}^{M\times M}$ is the unitary M-point DFT matrix.

It is readily checked that if the sequence of data frames $\{\boldsymbol{D}_q\}$ is zero-mean, proper and wide-sense stationary, then the sequence of transmit blocks $\{\boldsymbol{x}_m\}$ is zero-mean, proper and wide-sense cyclostationary (with period P), so the result from Theorem 1 can be applied in view of Remark 1 above. If, in addition, the entries of $\boldsymbol{D}_q$ are uncorrelated with unit variance, then $\mathbb{E}\{\boldsymbol{x}_m \boldsymbol{x}_{m-\ell}^H\} = \delta[\ell]\boldsymbol{I}_K$, so that the OTFS precoding operation does not modify the PSD with respect to CP-OFDM.

C. OQAM-FBMC

With the IFFT-based implementation [29, Sec. III-A], the OQAM-FBMC signal conforms to the structure of (1), with hop size $L = N/2$, and a common NP-length pulse $h_k[n] = h_0[n]$ for all active subcarriers. The transmit sequence $x_k^{(m)} \in \mathbb{C}$ is obtained from the *real-valued* data sequence $d_k^{(m)} \in \mathbb{R}$ as $x_k^{(m)} = d_k^{(m)} \mathrm{e}^{\jmath\frac{\pi}{2}(k+m)}$. Due to this, the vector sequence $\{\boldsymbol{x}_m\}$ is not proper in general, so that part (ii) in Assumption 1 does not hold, and Theorem 1 does not strictly apply.

VI. Examples

In the following examples the interpolation filter is assumed to be an ideal lowpass filter, i.e., $|H_{\mathrm{I}}(f)| = 1$ for $|fT_s| \le \frac{1}{2}$ and zero elsewhere. The analytical expressions have been validated by comparing them with the estimated PSD, which was obtained by applying Matlab's `pspectrum` tool to synthetic signals covering 10^6 blocks; no significant differences were observed in all cases.

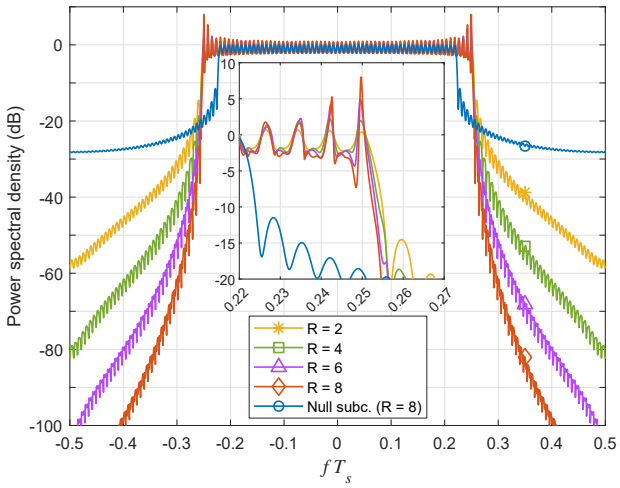

Fig. 1. PSD of R-continuous precoded OFDM.

A. R-continuous precoder

The scheme for R-continuous CP-OFDM proposed in [22] obtains the precoded sequence $\{\boldsymbol{x}_m \in \mathbb{C}^K\}$ from the data sequence $\{\boldsymbol{d}_m \in \mathbb{C}^D\}$, assumed zero-mean, uncorrelated, and proper, as $\boldsymbol{x}_m = \boldsymbol{B}\boldsymbol{d}_m + \boldsymbol{A}\boldsymbol{x}_{m-1}$, where $\boldsymbol{A} \in \mathbb{C}^{K\times K}$, $\boldsymbol{B} \in \mathbb{C}^{K\times D}$ are designed to impose $R = K - D$ continuity conditions, namely that of $s(t)$ and of its first $R-1$ derivatives, at the block boundaries. This precoder corresponds to a first-order, infinite impulse response LTI filter with transfer function $\boldsymbol{G}(f) = [\boldsymbol{I}_K - \mathrm{e}^{-\jmath 2\pi f T_s}\boldsymbol{A}]^{-1}\boldsymbol{B}$. The PSD is then given by $S_s(f) = \frac{1}{LT_s}|H_{\mathrm{I}}(f)|^2 \|\boldsymbol{G}^H(Lf)\boldsymbol{\phi}(f)\|^2$.

Fig. 1 shows the resulting PSD for a case in which $N = 128$, the CP length is $N/8$ (i.e., $L = \frac{9}{8}N = 144$), the pulse is rectangular as in (8), and the number of active subcarriers is $K = 65$, located at the passband center. Out-of-band emission is significantly reduced as the number of continuity conditions R increases, at the cost of some degradation in spectral efficiency (since the number of effective data subcarriers is $D = K - R$) and larger spectral peaks within the passband. The PSD of an unprecoded system with $K - 8 = 57$ active subcarriers is also shown for reference.

B. Edge windowing

In this case $\{\boldsymbol{x}_m\}$ is assumed zero-mean, uncorrelated, and proper, the IDFT size is $N = 4096$, the hop size is $L = \frac{9}{8}N = 4608$, and the number of active subcarriers is $K = 1025$, located at the passband center. These are divided into a group of $2S$ edge subcarriers (S at each passband edge) and a group of $K - 2S$ inner subcarriers. For each group, a raised cosine pulse is applied, with overlapping factors $Q_{\mathrm{edge}} = 80$ and $Q_{\mathrm{inner}} = 10$. For $S = 0$, this reduces to W-OFDM. The resulting PSD is shown in Fig. 2, together with that of a system with no windowing (i.e., using a rectangular pulse with no overlapping). Sidelobe suppression improves as the number of

This article has been accepted for publication in IEEE Communications Letters. This is the author's version which has not been fully edited and content may change prior to final publication. Citation information: DOI 10.1109/LCOMM.2022.3181728

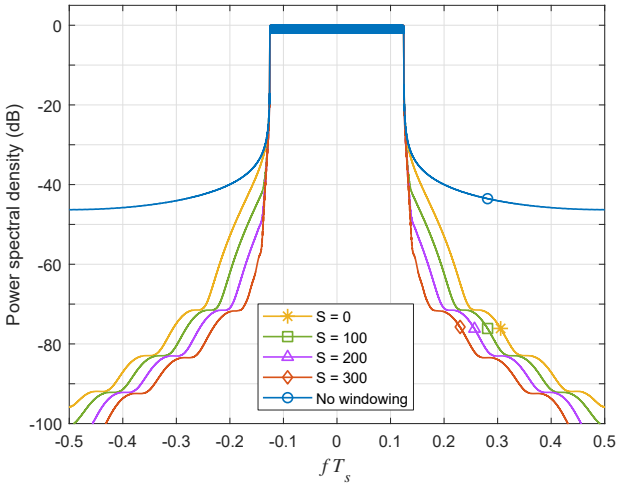

Fig. 2. PSD with edge windowing.

edge subcarriers S is increased, at the price of a reduced CP for edge subcarriers, and without generating spectral peaks.

VII. Conclusions

In this letter we have derived the exact expression for the PSD of multicarrier signals, allowing for inter-block correlation and subcarrier-specific pulse shaping. The only statistical assumptions adopted are the wide-sense cyclostationarity and properness of the vector-valued sequence modulating the active subcarriers. This expression is useful in order to evaluate the influence of system parameters as well as the performance of spectrum shaping techniques.

References

[1] R. Prasad, *OFDM for Wireless Communications Systems*. Norwood, MA, USA: Artech House, 2004.

[2] Z. You, J. Fang, and I. T. Lu, "Out-of-band emission suppression techniques based on a generalized OFDM framework," *EURASIP J. Adv. Signal Process.*, 2014, article ID 74 (2014).

[3] X. Huang, J. A. Zhang, and Y. J. Guo, "Out-of-band emission reduction and a unified framework for precoded OFDM," *IEEE Commun. Mag.*, vol. 53, no. 6, pp. 151–159, Jun. 2015.

[4] G. Cuypers, K. Vanbleu, G. Ysebaert, and M. Moonen, "Intra-symbol windowing for egress reduction in DMT transmitters," *EURASIP J. Adv. Signal Process.*, 2006, article ID 70387.

[5] M. T. Ivrlač and J. A. Nossek, "Influence of a cyclic prefix on the spectral power density of cyclo-stationary random sequences," in *Multi-Carrier Spread Spectrum 2007*. Dordrecht, The Netherlands: Springer, 2007, pp. 37–46.

[6] C. Liu and F. Li, "Spectrum modelling of OFDM signals for WLAN," *Electron. Lett.*, vol. 40, no. 22, pp. 1431–1432, Oct. 2004.

[7] J. Park, E. Lee, S.-H. Park, S.-S. Raymond, S. Pyo, and H.-S. Jo, "Modeling and analysis on radio interference of OFDM waveforms for coexistence study," *IEEE Access*, vol. 7, pp. 35 132–35 147, Jan. 2019.

[8] T. van Waterschoot, V. L. Nir, J. Duplicy, and M. Moonen, "Analytical expressions for the power spectral density of CP-OFDM and ZP-OFDM signals," *IEEE Signal Process. Lett.*, vol. 17, no. 4, pp. 371–374, Apr. 2010.

[9] J. F. Schmidt, D. Romero, and R. López-Valcarce, "Active interference cancellation for OFDM spectrum sculpting: Linear processing is optimal," *IEEE Commun. Lett.*, vol. 18, no. 9, pp. 1543–1546, Sep. 2014.

[10] R. Zayani, Y. Medjahdi, H. Shaiek, and D. Roviras, "WOLA-OFDM: A potential candidate for asynchronous 5G," in *2016 IEEE Global Commun. Workshops*, Dec. 2016, pp. 1–5.

[11] T. H. Pham, S. A. Fahmy, and I. V. McLoughlin, "Spectrally efficient emission mask shaping for OFDM cognitive radios," *Digital Signal Process.*, vol. 50, pp. 150–161, Mar. 2016.

[12] K. Hussain and R. López-Valcarce, "Optimal window design for W-OFDM," in *IEEE Int. Conf. Acoust., Speech, Signal Process. (ICASSP)*, 2020, pp. 5275–5289.

[13] A. Sahin and H. Arslan, "Edge windowing for OFDM based systems," *IEEE Commun. Lett.*, vol. 15, no. 11, pp. 1208–1211, Nov. 2011.

[14] C.-D. Chung, "Spectrally precoded OFDM," *IEEE Trans. Commun.*, vol. 54, no. 12, pp. 2173–2185, Dec. 2006.

[15] R. Xu and M. Chen, "A precoding scheme for DFT-based OFDM to suppress sidelobes," *IEEE Commun. Lett.*, vol. 13, no. 10, pp. 776–778, Oct. 2009.

[16] J. van de Beek, "Sculpting the multicarrier spectrum: a novel projection precoder," *IEEE Commun. Lett.*, vol. 13, no. 12, pp. 881–883, Dec. 2009.

[17] M. Ma, X. Huang, B. Jiao, and Y. J. Guo, "Optimal orthogonal precoding for power leakage suppression in DFT-based systems," *IEEE Trans. Commun.*, vol. 59, no. 3, pp. 844–853, Mar. 2011.

[18] J. Zhang, X. Huang, A. Cantoni, and Y. J. Guo, "Sidelobe suppression with orthogonal projection for multicarrier systems," *IEEE Trans. Commun.*, vol. 60, no. 2, pp. 589–599, Feb. 2012.

[19] J. F. Schmidt, S. Costas-Sanz, and R. López-Valcarce, "Choose your subcarriers wisely: Active interference cancellation for cognitive OFDM," *IEEE J. Emerg. Sel. Topics Circuits Syst.*, vol. 3, no. 4, pp. 615–625, Dec. 2013.

[20] R. Kumar, K. Hussain, and R. López-Valcarce, "Mask-compliant orthogonal precoding for spectrally efficient OFDM," *IEEE Trans. Commun.*, vol. 69, no. 3, pp. 1990–2001, 2021.

[21] J. van de Beek and F. Berggren, "N-continuous OFDM," *IEEE Commun. Lett.*, vol. 13, no. 1, pp. 1–3, Jan. 2009.

[22] Y. Zheng, J. Zhong, M. Zhao, and Y. Cai, "A precoding scheme for N-continuous OFDM," *IEEE Commun. Lett.*, vol. 16, no. 12, pp. 1937–1940, Dec. 2012.

[23] P. Wei, L. Dan, Y. Xiao, and S. Li, "A low-complexity time-domain signal processing algorithm for N-continuous OFDM," in *IEEE Int. Conf. Commun. (ICC)*, 2013, pp. 5754–5758.

[24] M. Mohamad, R. Nilsson, and J. van de Beek, "Minimum-EVM N-continuous OFDM," in *IEEE Int. Conf. Commun.*, May 2016, pp. 1–5.

[25] K. Hussain and R. López-Valcarce, "Memory tricks: Improving active interference cancellation for out-of-band power reduction in OFDM," in *Int. Workshop Signal Process. Adv. Wireless Commun. (SPAWC)*, 2021, pp. 86–90.

[26] H. G. Myung, J. Lim, and D. J. Goodman, "Single carrier FDMA for uplink wireless transmission," *IEEE Veh. Technol. Mag.*, vol. 1, no. 3, pp. 30–38, 2006.

[27] N. Michailow, M. Matthé, I. S. Gaspar, A. N. Caldevilla, L. L. Mendes, A. Festag, and G. Fettweis, "Generalized frequency division multiplexing for 5th generation cellular networks," *IEEE Trans. Commun.*, vol. 62, no. 9, pp. 3045–3061, Sep. 2014.

[28] A. Farhang, A. RezazadehReyhani, L. E. Doyle, and B. Farhang-Boroujeny, "Low complexity modem structure for OFDM-based orthogonal time frequency space modulation," *IEEE Wireless Commun. Lett.*, vol. 7, no. 3, pp. 344–347, Jun. 2018.

[29] R. Nissel, S. Schwarz, and M. Rupp, "Filter bank multicarrier modulation schemes for future mobile communications," *IEEE J. Sel. Areas Commun.*, vol. 35, no. 8, pp. 1768–1782, Aug. 2017.